Agricultural and Forest Meteorology 237 (2017) 18–29

Contents lists available at ScienceDirect

Agricultural and Forest Meteorology

journal homepage: www.elsevier.com/locate/agrformet

Influence of regional nighttime atmospheric regimes on canopy turbulence and gradients at a closed and open forest in mountain-valley terrain

S. Wharton[a,*], S. Ma[b], D.D. Baldocchi[b], M. Falk[c], J.F. Newman[d,1], J.L. Osuna[a], K. Bible[e,2]

[a] Atmospheric, Earth and Energy Division, Lawrence Livermore National Laboratory, Livermore, CA, USA
[b] Department of Environmental Science, Policy and Management, University of California, Berkeley, CA, USA
[c] Department of Land, Air and Water Resources, University of California, Davis, CA, USA
[d] School of Meteorology, University of Oklahoma, Norman, OK, USA
[e] College of the Environment, University of Washington, Seattle, WA, USA

ARTICLE INFO

Article history:
Received 12 October 2015
Received in revised form 26 January 2017
Accepted 29 January 2017

Keywords:
Fluxnet
Doppler lidar
Eddy covariance
Canopy turbulence
Mountain-valley wind
Friction velocity

ABSTRACT

Stable stratification of the nocturnal lower boundary layer inhibits convective turbulence, such that turbulent vertical transfer of ecosystem carbon dioxide (CO_2), water vapor (H_2O) and energy is driven by mechanically forced turbulence, either from frictional forces near the ground or top of a plant canopy, or from shear generated aloft. The significance of this last source of turbulence on canopy flow characteristics in a closed and open forest canopy is addressed in this paper. We present micrometeorological observations of the lower boundary layer and canopy air space collected on nearly 200 nights using a combination of atmospheric laser detection and ranging (lidar), eddy covariance (EC), and tower profiling instrumentation. Two AmeriFlux/Fluxnet sites in mountain-valley terrain in the Western U.S. are investigated: Wind River, a tall, dense conifer canopy, and Tonzi Ranch, a short, open oak canopy. On roughly 40% of nights lidar detected down-valley or downslope flows above the canopy at both sites. Nights with intermittent strong bursts of "top-down" forced turbulence were also observed above both canopies. The strongest of these bursts increased sub-canopy turbulence and reduced canopy virtual potential temperature (θ_v) gradient at Tonzi, but did not appear to change the flow characteristics within the dense Wind River canopy. At Tonzi we observed other times when high turbulence (via friction velocity, u_*) was found just above the trees, yet CO_2 and θ_v gradients remained large and suggested flow decoupling. These events were triggered by regional downslope flow. Lastly, a set of turbulence parameters is evaluated for estimating canopy turbulence mixing strength. The relationship between turbulence parameters and canopy θ_v gradients was found to be complex, although better agreement between the canopy θ_v gradient and turbulence was found for parameters based on the standard deviation of vertical velocity, or ratios of 3-D turbulence to mean flow, than for u_*. These findings add evidence that the relationship between canopy turbulence, static stability, and canopy mixing is far from straightforward even within an open canopy.

1. Introduction

Observations of ecosystem CO_2 source or sink magnitude (i.e., net ecosystem exchange of carbon, or *NEE*) come largely from surface flux towers which measure the turbulent vertical flux of CO_2 (F_c) between the vegetated surface and atmosphere with the eddy covariance (EC) technique. Nighttime F_c (i.e., ecosystem respiration flux) is frequently quality-controlled using the friction velocity (ustar or u_*) correction method, a procedure proposed by Goulden et al. (1996) as a way of reducing the systematic underestimation of nighttime respiration. This method uses the momentum flux variable u_* as a proxy for the magnitude of canopy turbulent exchange. This method assumes that each site has an identifiable u_* value (called the u_*critical threshold or u_{*crit}) beyond which the vertical transport of turbulence is considered sufficient for the EC system

* Corresponding author.
E-mail address: wharton4@llnl.gov (S. Wharton).
[1] Current affiliation: National Wind Technology Center, National Renewable Energy Laboratory, Golden, Colorado, USA.
[2] Current affiliation: Pacific Northwest Research Station, U.S. Forest Service, Washington, USA.

http://dx.doi.org/10.1016/j.agrformet.2017.01.020

to accurately measure F_c. Nighttime F_c which are determined to be made during times of poor vertical turbulent transport ($u_* < u_{*crit}$) are flagged and routinely replaced with modeled values based on an empirically-derived relationship between measured F_c and air or soil temperature taken during high u_* conditions, and at water-limited sites also with soil moisture.

Although the u_* correction method has been widely adopted by the Fluxnet community limitations to it have been explored and debated over the last decade. Some researchers have proposed alternative statistics to u_* to assess the strength of turbulent mixing within the canopy. Proposed metrics include the standard deviation of vertical wind speed (σ_W) (e.g., Acevedo et al., 2009; Thomas et al., 2013), ratio of σ_W to horizontal wind speed (U) (Thomas et al., 2013; Vickers and Thomas, 2013), ratio of a turbulent velocity scale (u_{TKE}) to U (Wharton et al., 2009), and a turbulence isotropy ratio (e.g., velocity aspect ratio, *VAR*) (Vickers and Mahrt, 2006; Vickers and Thomas, 2013).

Acevedo et al. (2009), for example, found that nights with little turbulent exchange can be misclassified as highly turbulent based on u_* if mesoscale transport is large in the atmosphere and captured in the averaging time window. This is due to the fact that the horizontal velocity variances ($\sigma^2{}_u$, $\sigma^2{}_v$) are sensitive to the chosen time-averaging scale. However, vertical velocity variance ($\sigma^2{}_w$) shows far less time dependence and may be a more accurate parameter under these conditions (Acevedo et al., 2009; Vickers and Thomas 2013). Likewise, Wharton et al. (2009) found a significant number of half-hours over small forest clear-cuts when u_* is high and suggested highly turbulent conditions, yet the ratio of a turbulent velocity scale to horizontal wind speed suggested that the horizontal advective flux may be significant in comparison to the vertical CO_2 exchange. Influences of mesoscale transport on *NEE* and on the calculation of u_* suggest that alternatives to the u_* correction method should be examined more widely.

Regional or mesoscale flows of relevance to EC tower sites include, but are not limited to, internal gravity waves, large-amplitude pressure waves, nocturnal low-level jets (LLJ), mountain/valley flow, and land/sea breezes. In addition, intermittent bursts of "top-down" forced turbulence have been commonly observed in the nocturnal boundary layer (e.g., Businger, 1973; Mahrt, 1989, 1999; van de Wiel et al., 2002; Acevedo and Fitzjarrald, 2003; Sun et al., 2012). These bursts can originate on clear, moderately stable nights from a variety of physical causes, including the breakdown of gravity waves (Acevedo and Fitzjarrald, 2003), from shear instability found underneath a LLJ (Karipot et al., 2008), from Kelvin-Helmholtz instabilities (Sun et al., 2012), from wind gusts aloft (Acevedo and Fitzjarrald, 2003), or from the interplay of radiative cooling and turbulent mixing (van de Wiel et al., 2002). Furthermore, data quality methodologies based on u_{*crit} or alternative turbulence parameters may remove meaningful EC tower measurements from the dataset if these turbulence bursts occur only sporadically, or if they occur at locations distant from the tower measurement point (Acevedo and Fitzjarrald, 2003).

One way to observe flow features found well above the canopy is to deploy a ground-based remote sensing instrument such as sound detection and ranging (sodar) or laser detection and ranging (lidar). Remote sensing devices extend the maximum measurement height by many hundreds of meters and the number of typical measurement levels at a flux tower site by a factor of ten or more. These instruments provide vertical profile measurements of wind in the lower atmosphere, including mean horizontal and vertical wind speed and direction up to a few hundreds of meters or more above ground level (a.g.l.). This range should be sufficient to measure most, if not all, of the nocturnal boundary layer.

A handful of researchers have deployed sodar (Thomas et al., 2006; Karipot et al., 2008; El-Madany et al., 2014) or lidar (Mann et al., 2008; Dellwik et al., 2010) at forest canopies. For example, Karipot et al. (2008) used sodar to observe LLJs far above (200–400 m a.g.l.) a Florida AmeriFlux pine canopy. Their observations showed a correlation between large nighttime F_c and LLJ activity, such that dynamically-generated turbulence found underneath strong jets was routinely transported downward into the forest canopy. This led to induced canopy mixing and the venting of large CO_2 fluxes to the top of the canopy at night.

Our present study is one of a handful to co-locate a wind profiling lidar and eddy covariance flux tower. Two locations were chosen for lidar deployment based on site differences in vegetative canopy structure, the likelihood of capturing non-local atmospheric events, and the richness of available micrometeorological instruments. We note that the term non-local here refers to atmospheric scales of interest on the order of hundreds of meters to tens of kilometers, and from minutes to hours.

We chose the Wind River AmeriFlux site to study flow dynamics and canopy exchange within and above a tall, high biomass, needleleaf forest. The Tonzi AmeriFlux site provided a location to study flow features within and above an open, oak-grass savannah. Flow at both towers in the warmer months is influenced by strong thermal gradients induced by synoptic weather patterns (e.g., the summer-time North Pacific High) and regional mountain-valley terrain. This study is motivated by the fact that micrometeorological interactions between large-scale flow circulations, local terrain slopes, and canopy density and roughness remain poorly understood (e.g., Froelich and Schmid, 2006; Rotach et al., 2008; Wang et al., 2015). We address this uncertainty by including wind profiles taken in the nocturnal boundary layer to identify non-local flow features along with the more traditional above canopy and sub-canopy EC datasets at two sites with different canopy structures.

Specific goals were to: (1) identify and categorize dominant, non-local, above-canopy, nocturnal atmospheric phenomena by type and strength using the lidar wind profiles, (2) calculate wind flow and turbulence (e.g., *TKE*, wind shear, u_*, σ_W) statistics according to atmospheric phenomenon to look for any atmospheric or canopy-related trends, (3) compare the utility of using various nighttime turbulence filters (e.g., u_*, σ_W, etc.) to estimate vertical canopy mixing under different atmospheric phenomena events at an open and closed canopy, and (4) evaluate the overall utility of co-locating a remote sensing device (here we used lidar) at woodland/forested flux tower sites.

2. Site description

Wind River AmeriFlux tower (45.8205, −121.9519, 371 m a.s.l.) is located in a 500-ha, high biomass, evergreen needleleaf forest in the southern Cascade Range of Washington State, USA. The stand has never been managed and is thought to have originated after a natural fire around the year 1500. Old-growth characteristics include the presence of large, live old trees, a deep (50 m +) vertically continuous canopy, large snags, and large amounts of coarse woody debris on the forest floor (Harmon et al., 2004). The stand has eight conifer species and is dominated by Douglas-fir (*Pseudotsuga menziesii* (Mirbel) Franco) and western hemlock (*Tsuga heterophylla* (Raf.) Sarg). Mean canopy height (h_c) is approximately 50–55 m. Stand density is approximately 427 trees per hectare, tree ages range from 0 to ∼500 years (Shaw et al., 2004), and total leaf area index (*LAI*) estimates range from 8.2 to 9.2 m^2/m^2 with little seasonality (Thomas and Winner, 2000; Parker et al., 2002). The understory has a *LAI* of 1.69 m^2/m^2 (Thomas and Winner, 2000) and is dominated by vine maple (*Acer circinatum*) salal (*Gautheria shallon*), Oregon grape (*Berberis nervosa*), and bracken fern (*Pteridium aquilinum*). Mean annual air temperature is 8.8°C and total water-year precipitation is 2325 mm.

Tonzi Ranch AmeriFlux tower (38.4318, −120.9668) is located in the lower foothills of the Sierra Nevada, California, USA, at an elevation of 177 m a.s.l. The study area is dominated by an open canopy of deciduous blue oak (*Quercus douglasii*), which cover roughly 40% of the landscape, and interspersed gray pine (*Pinus sabineana*). Average *LAI* for the tree canopy is $0.71 \pm 0.41\ m^2/m^2$, mean h_c is 9.41 ± 4.33 m, and average tree diameter at breast height (dbh) is 0.22 m (Baldocchi et al., 2010; Ryu et al., 2010). The understory and open meadows are dominated by cool-season C3 grasses (*Brachypodium distachyon, Hypochaeris glabra, Bromus madritensis*) which are grazed by cows in the winter and spring. The oak savannah is a two-layered system: grasses dominate *NEE* in the wet winter, trees and grasses dominate *NEE* in the spring following bud break (typically in March), and trees dominate *NEE* in the summer when moisture limitations cause the grasses to senesce. Mean annual temperature is 16.5 °C; mean annual precipitation is 562 mm.

Both sites are in locations subject to terrain-influenced, mountain-valley flow. Wind River is located towards the north end of a 23 km long valley which emerges into the Columbia River Gorge about 15 km south of the tower (Fig. 1a). While the local slope in the immediate tower footprint is less than 4%, steeper slopes rise approximately 1500 m above the valley floor on both sides. The tower is located between two major topographical features: Bunker Hill (730 m elevation) to the southeast and Trout Creek Hill (895 m elevation) to the northwest. Strong differential heating between the Cascade Mountains and Wind River Valley creates along-axis, diel flow in the valley in warmer months. These mountain-valley winds are characterized by a diel wind reversal: stronger up-valley, southeasterly flow occurs during the day and weaker down-valley, northwesterly flow occurs at night (Fig. 1b).

The local fetch at Tonzi Ranch is relatively flat; however, the terrain becomes increasingly complex in the easterly direction towards the Sierra Nevada Range (Fig. 1c). Regionally strong differential heating between the Sacramento Valley and nearby mountains creates cross-axis, diel flow (Morgan and Slusser, 1978). These mountain-valley flows include upslope winds from the westerly-northwesterly direction during the day and downslope winds from the easterly-southeasterly direction overnight (Fig. 1d).

3. Materials and methods

3.1. Flux towers

The eddy covariance datasets contained measurements of mass, energy, velocity and momentum averaged over 30-min. The data were screened by wind direction to remove times when the tower wake may have influenced turbulence measurements or times when the tower footprint extended beyond the ecosystem of interest. The latter was a concern only for Wind River where younger Douglas-fir stands are found to the north and east. Both sites have long records of continuous EC measurements: Wind River since 1998 (Paw U et al., 2004; Falk et al., 2005, 2008; Wharton et al., 2012) and Tonzi since 2001 (Xu and Baldocchi, 2003; Baldocchi et al., 2006; Ma et al., 2007). Full instrumentation and data processing details are found in the above citations and are briefly described here.

Tonzi Ranch has two EC flux towers instrumented each with an open path gas analyzer (LI-7500, LI-COR, Lincoln, NE, USA) and 3-D sonic anemometer (Gill WMP 1352, Gill Instruments Limited, Hampshire, UK). The understory tower has instruments at 2 m a.g.l. or 0.2 h_c; the overstory tower's instruments are placed above the oak canopy at a height of 23 m a.g.l or 2.5 h_c. The understory tower measures vertical flux exchanges over the grasses and soil, while the overstory tower measures over the entire ecosystem including the tree canopy. The site also has a vertical profile of mean CO_2 concentration (*[CO_2]*, ppm) mounted along the overstory tower. [CO_2] is measured at 0.35 m, 1.8 m, 6.0 m, and 23.5 m a.g.l., at a 30-min interval per height using a H_2O/CO_2 gas analyzer (LI-820, LI-COR).

At Wind River, EC measurements are taken approximately 15 m above the conifer canopy at a height of 67 m a.g.l. or 1.2 h_c using a 3-D sonic anemometer (CSAT3, Campbell Scientific Inc., Logan, UT, USA) and closed path infrared gas analyzer (LI-7000, LI-COR). Wind River also has a profiling system installed along the flux tower and *[CO_2]* is measured using a CO_2 isotope analyzer (G2131-i analyzer, Picarro, Santa Clara, CA, USA) once to twice an hour at three heights: just above the forest floor (z = 0.5 m), near the bottom of the canopy crown (z = 10 m), and above the canopy (z = 67 m). At 2 m a forest floor meteorological station also measures horizontal wind speed (*U*, m/s), wind direction (°), air temperature (T_a, °C), and relative humidity (*RH*, %).

3.2. Wind lidar campaigns

The Wind Cube v2 (Leosphere, Orsay, France) is a pulsed lidar and uses regularly spaced emissions of light for a specified pulse length to measure the radial wind component using a Doppler Beam Swinging (DBS) technique (Strauch et al., 1984). The DBS scan alternately uses consecutive beams off-zenith (cone half-angle of 28°) in the north, east, south and west directions, followed by a vertically pointing beam, with a constant range gate size of 20 m (Cariou and Boquet, 2011). Measurements are taken at a sampling rate of approximately 0.25 Hz (4 s) to complete a full DBS scan, however the Wind Cube v2 actually calculates *u*, *v*, and *w* at a faster frequency (1 Hz) using the current radial velocity and the radial velocity from the previous four beam locations. The lidar has an accuracy of ± 0.1 m/s for *U* and 1.5° for wind direction in ideal conditions (e.g., stationarity, flat terrain, horizontally homogenous flow). Accuracy in complex terrain is reduced but still estimated to be within 3–5% based on extensive testing (Krishnamurthy and Boquet, 2014).

In one campaign we also used a ZephIR 300 (ZephIR Ltd., North Ledbury, UK). The ZephIR is a continuous wave lidar and uses a multi-beam circular scan (also called a velocity-azimuth display scan or VAD) to deduce properties of the wind field (Slinger and Harris, 2012). One scan is taken every second with 50 measurements per scan at a cone half-angle of 30°. Each measurement height is taken in sequence such that it takes ~15 s to resample any given height. The range gate varies from 1.4 m at 10 m to 15.4 m at 100 m a.g.l. In ideal conditions, measurement error is <0.5% for *U* and <0.5° for wind direction.

While a measure of turbulence can be extracted from high frequency lidar data it is important to note that these measurements differ slightly from those collected with a 3-D sonic anemometer. Lidar's larger sample volume, slower sampling frequency, and for the DBS and VAD techniques, possible cross-contamination by the wind components can lead to differences in the *u*, *v* and *w* variances (e.g., Sathe and Mann, 2013; Newman et al., 2016). However, while 3-D turbulence from a lidar is not exactly the same as measured by a 3-D sonic anemometer, the spectral energy captured by lidar appears to be approximately the same as that measured by a 3-D sonic at low wave numbers ($k < 0.005\ m^{-1}$) before the effects of spatial averaging begin to dominate (Sathe and Mann, 2012). Accuracy for energy scales at the highest frequency range (e.g., >0.25 Hz) is less certain (Cañadillas et al., 2010; Sathe and Mann, 2012), but appears to be most prone to error during unstable conditions due to velocity cross-contamination (Newman et al., 2016).

The Windcube v2 was used in four of five field campaigns: Wind River in May 2012 and July-October 2013, and Tonzi in April 2012 and August-November 2012. The ZephIR 300 was used at Tonzi in April-May 2013. From the high frequency *u*, *v* and *w* data (1 Hz for

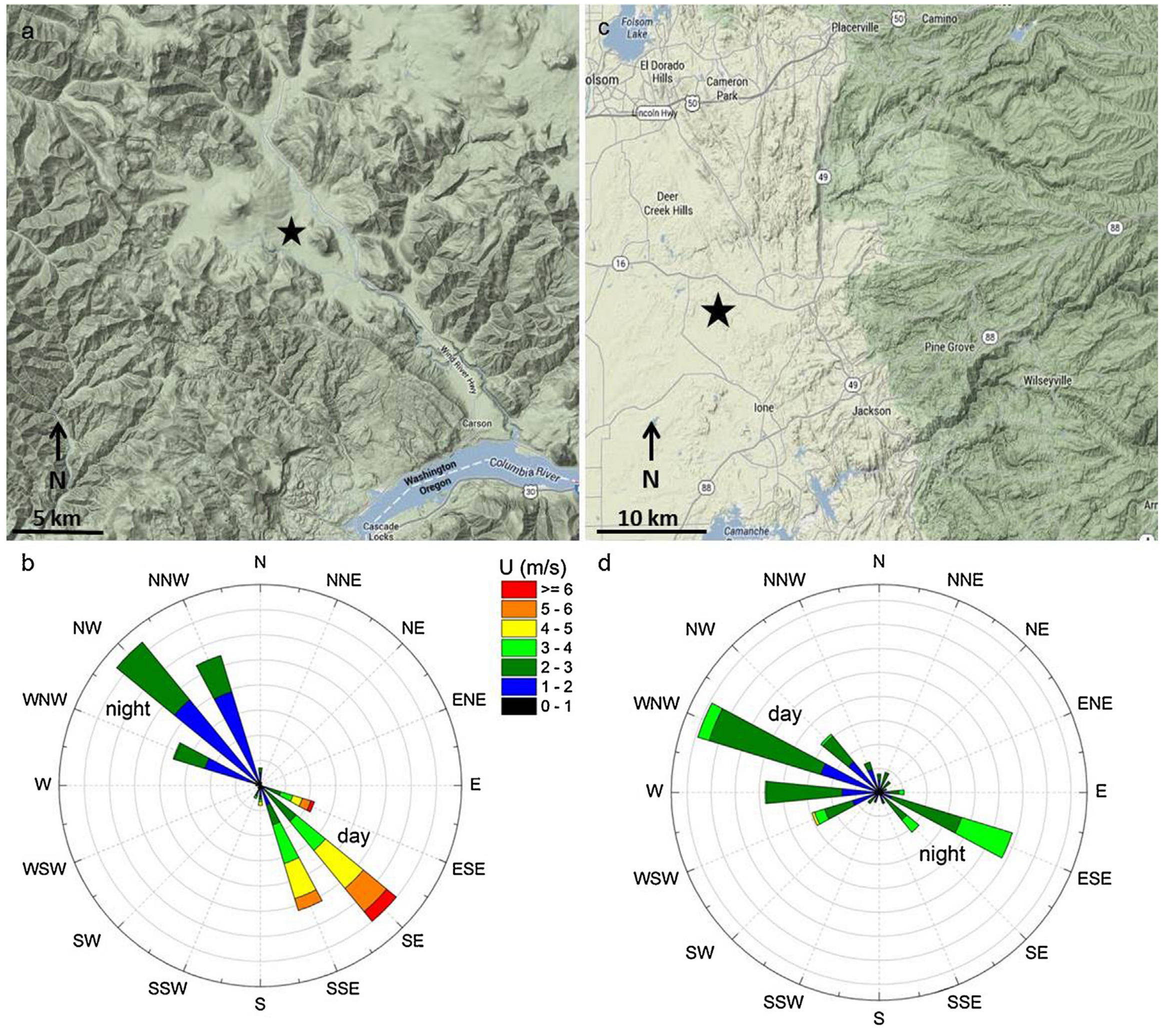

Fig 1. Topographical relief map of the region surrounding (a) Wind River AmeriFlux tower in southern Washington and (c) Tonzi Ranch AmeriFlux tower in northern California. Tower locations are shown with a star. Overstory wind direction and wind speed is shown for (b) Wind River and (d) Tonzi by time of day. Both sites experience diel valley-mountain flow.

Table 1
Lidar field campaign details.

Site	Campaign dates	Lidar	Measurement heights	Dominant vegetation	Ecosystem characteristics
Tonzi Ranch	April 5–26, 2012	Wind Cube v2	40–200 m at 20 m intervals	Deciduous oak, grass understory	Oak bud-break in late March, photosynthesizing grass canopy.
Tonzi Ranch	Aug. 24-Nov. 2, 2012	Wind Cube v2	40–150 m at 10 m intervals	Deciduous oak, grass understory	Summer drought stress on oaks, non-photosynthesizing grass canopy.
Tonzi Ranch	April 3-May 28, 2013	ZephIR 300	10–100 m at 10 m intervals	Deciduous oak, grass understory	Oak bud-break in late March, photosynthesizing grass canopy.
Wind River	May 1–11, 2012	Wind Cube v2	40–200 m at 20 m intervals	Evergreen conifer	Period of high net carbon uptake.
Wind River	July 11-Oct. 29, 2013	Wind Cube v2	40–100 m at 10 m intervals, 120–200 m at 20 m intervals	Evergreen conifer	Period of summer drought stress on tall conifers and attenuated carbon uptake.

Wind Cube v2, every ~15 s for ZephIR 300), 30-min averages of *U*, *w*, direction, and *TKE* were calculated. A carrier-to-noise ratio threshold of −23 was used to compute the half-hourly averages for the Wind Cube v2. This removed half-hourly data points with high noise signals. Nights with recorded precipitation were also removed from the analysis. This left a total of 80 nights at Wind

River and 113 nights at Tonzi. We intended to deploy the lidar on the forest floor at Wind River; however, we were unable to find a gap large enough in the dense, tall forest to prevent obstruction of the laser beams to retrieve an unperturbed measurement. Therefore, the lidar was placed in a clearing just outside the stand approximately 450 m south of the flux tower. At Tonzi large gaps between the trees allowed us to place the lidar directly within the canopy 100 m northwest of the flux tower. Complete lidar campaign details are listed in Table 1.

3.3. Turbulence parameters

Four parameters were evaluated for estimating the magnitude of canopy turbulence mixing strength. Each is based on 3-D sonic anemometer data. The set included friction velocity (u_*), the standard deviation of vertical wind speed (σ_w), a *TKE* velocity-scaled intensity (I_{TKE}), and the gradient Richardson number (Ri_{gr}). u_* (m/s) is defined in Eq. (1),

$$u_* = \left(\overline{u'w'}^2 + \overline{v'w'}^2\right)^{1/4} \tag{1}$$

where $\overline{u'w'}$ and $\overline{v'w'}$ are the stream-wise and cross-wise momentum fluxes (m^2/s^2). For reference, site-specific u_* critical thresholds are 0.2 m/s and 0.1 m/s, respectively, at Wind River (Falk et al., 2005) and Tonzi (Ma et al., 2007). σ_w (m/s) is defined in Eq. (2),

$$\sigma_w = \left(\overline{w'w'}\right)^{1/2} \tag{2}$$

where $\overline{w'w'}$ is variance of vertical wind speed (m^2/s^2). Because Tonzi has two flux towers we were also able to calculate the ratio of σ_w measured at the understory station to σ_w measured above the canopy, ($\sigma_{wunderstory}/\sigma_{woverstory}$).

I_{TKE} is defined in Eq. (3):

$$I_{TKE} = \frac{u_{TKE}}{\overline{U}}, \tag{3}$$

where $\overline{U}$ is mean horizontal wind speed (m/s) and a turbulence velocity scale (u_{TKE}) (m/s) is defined in Eq. (4):

$$u_{TKE} = \left(0.5(\overline{\sigma_u^2} + \overline{\sigma_v^2} + \overline{\sigma_w^2})\right)^{1/2} = (TKE)^{1/2} \tag{4}$$

I_{TKE} is a modified form of the turbulence intensity parameter (I_U) presented in Wharton et al. (2009). I_{TKE} is used to determine conditions when mass transport by mean horizontal flow may be significant compared to the transport of mass through turbulent eddy flow. This parameter assumes that the efficiency of turbulence to transport mass and energy can be represented by the magnitude of *TKE*. As shown in Wharton et al. (2009) I_{TKE} is a well suited turbulence parameter for landscapes where horizontal advection of CO_2 may be a significant or non-negligible portion of *NEE*, e.g., sites in complex terrain or ones with abrupt canopy roughness changes.

Ri_{gr} is defined in Eq. (5),

$$Ri_{gr} = \frac{\dfrac{g}{\overline{\theta_v}}\dfrac{\partial\overline{\theta_v}}{\partial z}}{\left[\left(\dfrac{\partial\overline{U}}{\partial z}\right)^2 + \left(\dfrac{\partial\overline{v}}{\partial z}\right)^2\right]} \tag{5}$$

where g is the acceleration due to gravity (m/s^2), $\overline{\theta_v}$ is mean virtual potential air temperature (K), z is measurement height (m), and u and v are the stream-wise and cross-wise wind velocities (m/s). Gradients of wind speed and temperature were calculated from measurements taken at the overstory and understory EC towers at Tonzi, and at Wind River using the overstory EC and forest floor meteorological stations. Ri_{gr} is often used to determine dynamic stability in a statically stable atmosphere. An atmosphere is described as dynamically stable if R_{igr} is greater than a turbulence threshold (R_T). This represents conditions when turbulent flow becomes largely non-turbulent due to the enhancement of stable stratification following surface cooling. Dynamically unstable conditions occur as non-turbulent flow becomes turbulent, possibly due to the buildup of wind shear and resultant Kelvin-Helmholtz instability. When R_{igr} is less than a critical threshold (R_c) the onset of turbulence is predicted to occur. Following Stull (1988) thresholds of R_T = 1.0 and R_c = 0.25 were used.

3.4. Atmospheric phenomena

Dominant, nighttime, non-local atmospheric phenomena events were identified from the lidar wind profiles and separated into two groups. The first group included topography-induced, mountain-valley flows: downslope winds at Tonzi and down-valley winds at Wind River. The second group was defined by the presence of intermittent, sporadic bursts of “top-down” forced turbulence originating far above the canopy. Here we differentiate between intermittent, non-local turbulence generated aloft, from intermittent, local, high-frequency random turbulence motions and identify the first.

The intensity of the downslope/down-valley flow was determined by the magnitude of wind shear found between the nose of the wind jet (z_{jet}) and a height aloft (z_{aloft}) (here, we used z_{aloft} = 120 m as it was the highest height from the lidar with nearly 100% available wind speed data). A downslope/down-valley flow was classified as strong if the shear ratio was greater than 1.5. Strong top-down turbulence events were identified when the ratio between *TKE* measured during turbulence bursts to alternating calm periods during the course of a night was greater than 1.5 at z = 2 h_c. Half-hours that met these criteria because of very weak winds or very low *TKE* levels were screened and removed from the analysis.

4. Results and discussion

4.1. Mountain-valley flow characteristics

On nights with down-valley flows, a diel reversal of the wind direction (SE-NW) was observed above the Wind River forest canopy commencing after dusk. These events occurred on 43% of the lidar campaign nights. Of these, 34% were classified as strong events. Sky conditions on these nights were clear and followed strong daytime differential heating between the valley floor and surrounding mountain slopes. A weak jet with a maximum velocity of 1.5–3.0 m/s (U_{jet}) was observed at heights of 70–100 m a.g.l. (z_{jet}), or 1.2–1.8 times the canopy height (Fig. 2, Table 2) during strong down-valley flow events. For comparison, these characteristics are similar to those observed (z_{jet} = 2.3 h_c, U_{jet} = 1–3 m/s) over a forested mountain valley in Northeast China (Wang et al., 2015).

Downslope flows at Tonzi were observed on 37% of the field campaign nights. These flows were almost exclusively from the east-southeast and of these 35% were classified as strong events. Strong downslope flows were observed farther above the oak canopy (z_{jet} = 30–70 m a.g.l. or 3–7 h_c) and contained stronger jet velocities (U_{jet} = 4.0-7.5 m/s) than the down-valley flows observed at Wind River (Fig. 2, Table 2). Other studies have measured downslope flows much closer to the ground (z_{jet} = 5–15 m a.g.l.), but those observations were made at sites with greater slopes than found at Tonzi (e.g., Pyles et al., 2004; Yi et al., 2005; Whiteman and Zhong, 2008; Choi et al., 2011; Smith and Porté-Agel, 2014). For example, downslope flows at the Niwot Ridge AmeriFlux site (slope = 5-7%) are typically observed in the forest sub-canopy (z_{jet} = 4 m a.g.l.), well

Table 2
Characteristics of downslope or down-valley flow circulations.

Site	Type	z_{jet} range	U_{jet} range	Strong shearing stress observed below jet	Percentage of lidar campaign nights
Tonzi Ranch	Cross-axis, downslope	30–70 m or 3–7 h_c	4.0–7.5 m/s	Yes	37%
Wind River	Along-axis, down-valley	70–100 m or 1–2 h_c	1.5–3.0 m/s	No	43%

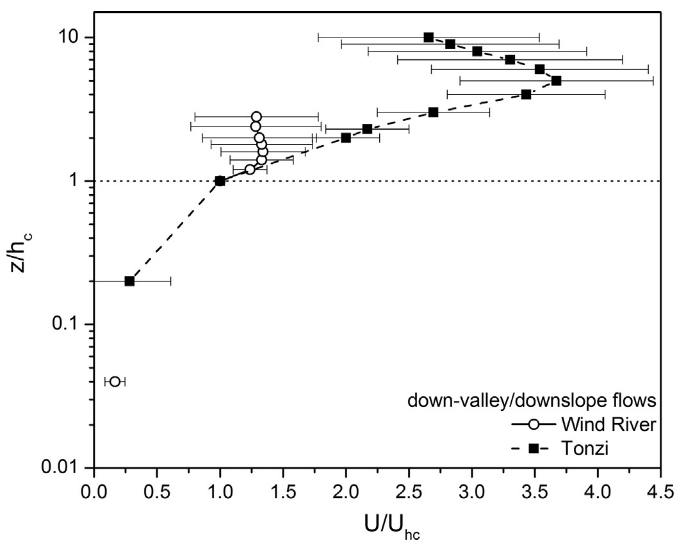

Fig. 2. Mean vertical profiles of horizontal wind speed (U) normalized by canopy height (h_c) during strong nighttime down-slope or downvalley flow events during the lidar campaign period. Note the strength of the mean downslope jet at Tonzi. Measurements were taken with sonic anemometry and lidar. The dotted line is drawn at mean canopy height. Error bars are ± one standard deviation.

below the overstory EC station (Yi et al., 2008). Given the gentler slope at Tonzi and farther distance from the mountains, our downslope jet height measurements agree better with field study observations that show that jet height increases with increasing downslope distance (Stull 1988).

Figs. 3 and 4 show a 24-h period at Wind River and Tonzi with typical strong down-valley and downslope flow events. Down-valley winds at Wind River are associated with weak downward vertical wind velocities, a weak horizontal jet near the top of the canopy, and very low values of nocturnal boundary layer *TKE* and overstory u_* (Fig. 3). Elevated values of *TKE* produced by a shear stress found underneath the jet were not observed at Wind River and u_* (mean = 0.11 m/s) remained well below the site's u_* critical value ($u_* < 0.2$ m/s) on these nights. The virtual potential temperature gradient ($\Delta\theta_v/\Delta z = (\theta_{v67} - \theta_{v2})/(z_{67} - z_2)$) indicated that the dense canopy was less statically stable during the nighttime hours than during the daytime, even though u_* and *TKE* show higher values at the top of the canopy during daylight hours, suggesting a potential mechanism for daytime canopy mixing. Strong daytime canopy inversions have been observed before in dense, high *LAI* forest stands including Wind River (Pyles et al., 2004) and others in the Pacific Northwest (Thomas et al., 2013). Thomas et al. (2013) attribute this to daytime radiative heating in the upper canopy which results in a large thermal gradient between the overstory and understory. This gradient may produce a weak stably stratified canopy which acts to suppress turbulence. At night, however, radiative cooling in the upper canopy reduces the temperature gradient (Thomas et al., 2013). However, it must be stressed that since our potential temperature gradient was based only on two heights, we may have missed the measurement of temperature inflection points found within the canopy, such as those observed in Pyles et al. (2004) when the tower was more robustly equipped with a profile of multiple temperature sensors.

In contrast to Wind River, nighttime $\Delta\theta_v/\Delta z$ at Tonzi is enhanced indicating a more stable nocturnal boundary layer or stronger surface temperature inversion (Fig. 4). In open canopies this occurs when the sub-canopy air space is strongly stratified, partially due to strong radiative cooling of the ground between the trees (van de Wiel et al., 2002). Differences at Tonzi also included stronger downward vertical wind velocities, a stronger horizontal wind jet, larger *TKE* values found underneath the jet, and elevated overstory u_* during downslope flows. Enhanced wind shear underneath a downslope jet can create a significant shear stress. At Tonzi this shear stress appears to develop at the height of the overstory EC station and is observed as elevated u_* at the overstory 3-D sonic anemometer. Mean overstory u_* during strong downslope flows (n = 15 nights) was 0.23 m/s and well above the site's threshold for determining times of adequate turbulence conditions (u_{*crit} = 0.1 m/s).

4.2. Top-down forced turbulence characteristics

Top-down forced turbulence nights were characterized as having strong intermittent bursts of turbulence, generally occurring one to three times a night and each lasting 30 min to 3 h, during an otherwise calm, stable night. At both Tonzi and Wind River the turbulence bursts appear to be produced by enhanced wind shear caused by strong intermittent wind gusts originating far above the canopy and beyond the maximum height range of our lidars. Nights with strong top-down forced turbulence are shown in Fig. 5 for Wind River and Fig. 6 for Tonzi. The top-down forced turbulence events were detected in the overstory u_* data record at both sites. Peaks in overstory u_* coincided directly in time with elevated values of lidar *TKE* and wind shear found well above the canopy ($z = 2\,h_c$), and in many cases, also with strong downward vertical wind velocities in the lower boundary layer.

At Wind River enhanced values of u_* and σ_w, measured just above the canopy during turbulent bursts, did not coincide in time with any observable changes in canopy $\Delta\theta_v/\Delta z$ (Fig. 5), or with understory wind speed. Furthermore, [CO_2] profile measurements taken at 0.5, 10 and 67 m along the tower showed no indication that turbulent bursts reached depths down to 10 m, as there were no discernable differences in the sub-canopy (z = 10–0.5m) or canopy (z = 67–10 m) [CO_2] gradients during half hours containing turbulence bursts compared to nonevent half-hours. Any gradient changes that occurred in the mid-canopy were unfortunately missed by our 3-point sampling setup. Due to the lack of high resolution canopy measurements at Wind River the remainder of the paper will focus on canopy flows at the open canopy Tonzi site.

At Tonzi a reduction in canopy $\Delta\theta_v/\Delta z$ was observed during turbulence burst events (Fig. 6) and was likely caused by the downward transport of warmer air from aloft reaching the understory (2 m) station. This observation is similar to that reported by Acevedo and Fitzjarrald (2003) who found that strong wind gusts promote surface layer mixing with the upper boundary layer, warming the surface layer from aloft. Evidence for these bursts reaching the understory station was also found in the half-hourly wind data as we measured greater values of u_* and σ_w at 2 m during these events. For example, understory u_* often exceeded the criteria threshold set for u_* at the overstory station during top-down forced turbulent burst events.

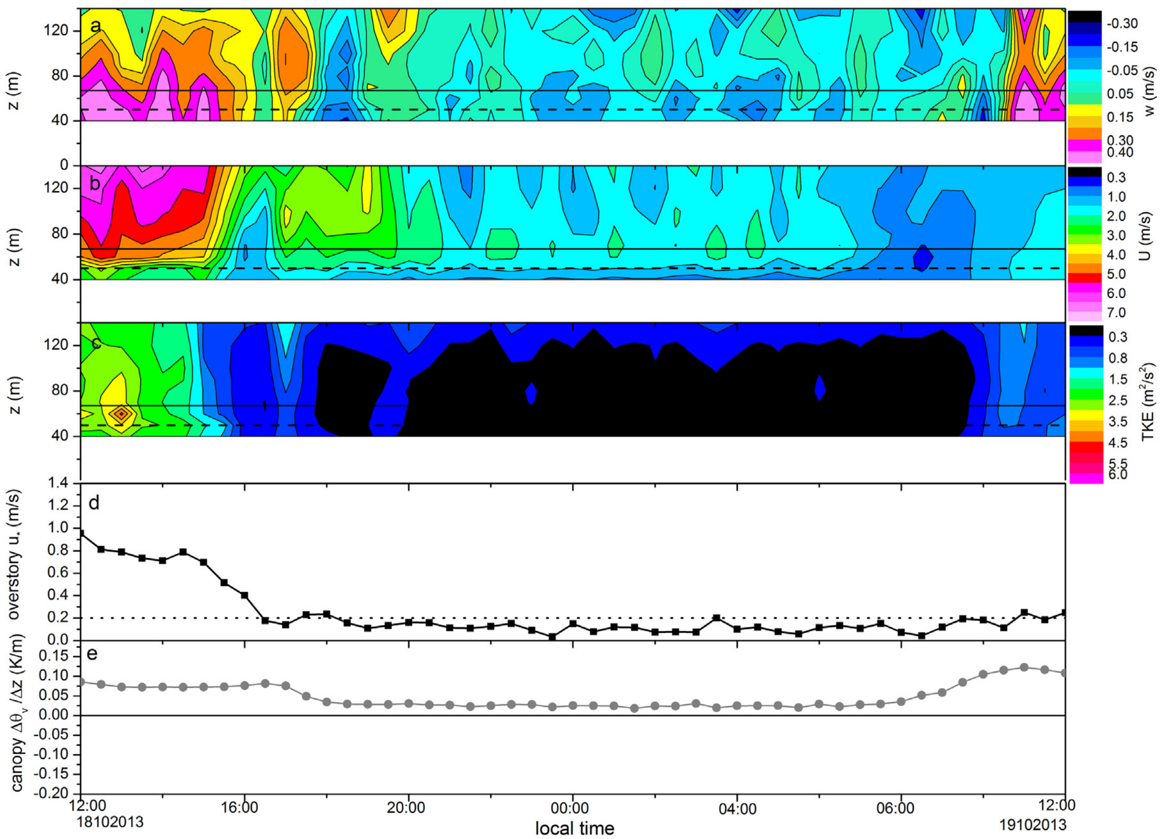

Fig. 3. A typical nocturnal down-valley flow event at Wind River shown for the night of 18–19 October 2013. Note that time is plotted starting at midday (12:00 local time) to highlight the nighttime hours in the middle of the time series. Plotted are (a–c) color contours of measured vertical wind speed (w), horizontal wind speed (U), and turbulence kinetic energy (*TKE*) from z = 40–140 m, (d) overstory ustar (u_*), and (e) canopy gradient of virtual potential temperature ($\Delta\theta_v/\Delta z$) between the overstory and forest floor. The dotted horizontal line in (a-c) is drawn at mean canopy height; the solid line shows the height of the EC overstory measurement. The dotted line in (d) indicates $u_{*\mathrm{crit}}$.

4.3. Turbulence parameters for estimating flow coupling/decoupling

In Fig. 7 we evaluate the magnitudes of the four turbulence parameters by wind direction at Tonzi. This plot reveals that turbulence parameter values are largely dependent by whether or not they were measured during a narrow wind direction range corresponding to 90° to 135° or ESE. While the use of lidar during our field campaigns determined that these winds corresponded to downslope events, this observation is significant because it indicates that downslope events can largely be identified by wind direction alone from the EC tower. We also use this plot to identify thresholds for two of our turbulence parameters, $\sigma_{wunderstory}/\sigma_{woverstory}$ and I_{TKE}. For both parameters the median value was chosen to be the threshold, as this value appeared to segregate the two nighttime atmospheric events. U_* and R_{igr} thresholds are based on published values as described in Section 3.3.

In Fig. 7a, 73% of the half-hours measured during downslope flow had u_* values greater than $u_{*\mathrm{crit}}$ (>0.1 m/s), and 21% of those half-hours had $u_* > 0.3$ m/s. For comparison, u_* values greater than 0.3 m/s occurred less than 5% of the time during strong top-down forced turbulence events. Downslope flows were generally associated with smaller values of $\sigma_{wunderstory}/\sigma_{woverstory}$ (Fig. 7b). Smaller ratios indicate half-hours when understory σ_w is much smaller in magnitude than values measured in the overstory, suggesting stronger canopy decoupling. Higher σ_w ratios suggest either elevated σ_w at the bottom of the canopy (such that values approach overstory σ_w), or conditions when weak vertical variance is found in both the top and bottom layers of the canopy. Elevated understory σ_w appears to be driving the Tonzi σ_w ratios during top-down forced turbulence events. This is similar to findings by Thomas et al. (2013) who discuss the utility of using sub-canopy σ_w for predicting the canopy coupling/decoupling regime.

I_{TKE} values were generally lower during downslope flows than during top-down forced turbulence events (Fig. 7c). This indicates that during downslope flow, 3-D turbulence is relatively small compared to the mean horizontal wind speed. If a horizontal CO_2 gradient is present, these conditions may create a possible violation of one of the major assumptions in the simplified 1-D EC mass balance equation for *NEE*. This is the assumption that the horizontal advection flux can be considered negligible compared to the vertical turbulent transport of carbon.

The gradient Richardson number at Tonzi shows that the nighttime half-hours are always statically stable ($R_{igr} > 0$) in the open canopy regardless of atmospheric phenomena (Fig. 7d). Furthermore, Ri_{gr} was always above the critical value ($R_c = 0.25$) during downslope flows, suggesting that the nocturnal boundary layer was not dynamically unstable during these events. In fact, nearly 50% of the downslope flow half-hours were determined to be dynamically stable ($R_{igr} > R_T$), while dynamically unstable conditions were frequently observed during top-down forced turbulence events.

During downslope flows, the canopy is both more dynamically stable (as shown by R_{igr} in Fig. 7d) and more strongly stratified (as suggested by θ_v gradients, mean $\Delta\theta_v/\Delta z = 0.24$ K/m) than during top-down forced turbulence events (mean $\Delta\theta_v/\Delta z = 0.11$ K/m) (Fig. 8). We make the assumption here that a larger potential temperature gradient in the open canopy suggests increasing static stability, and the possibility of flow decoupling between the sub-canopy and above-canopy air space when $\Delta\theta_v/\Delta z$ is above 0.15 K/m. This threshold is equal to the value of the 1st Quartile

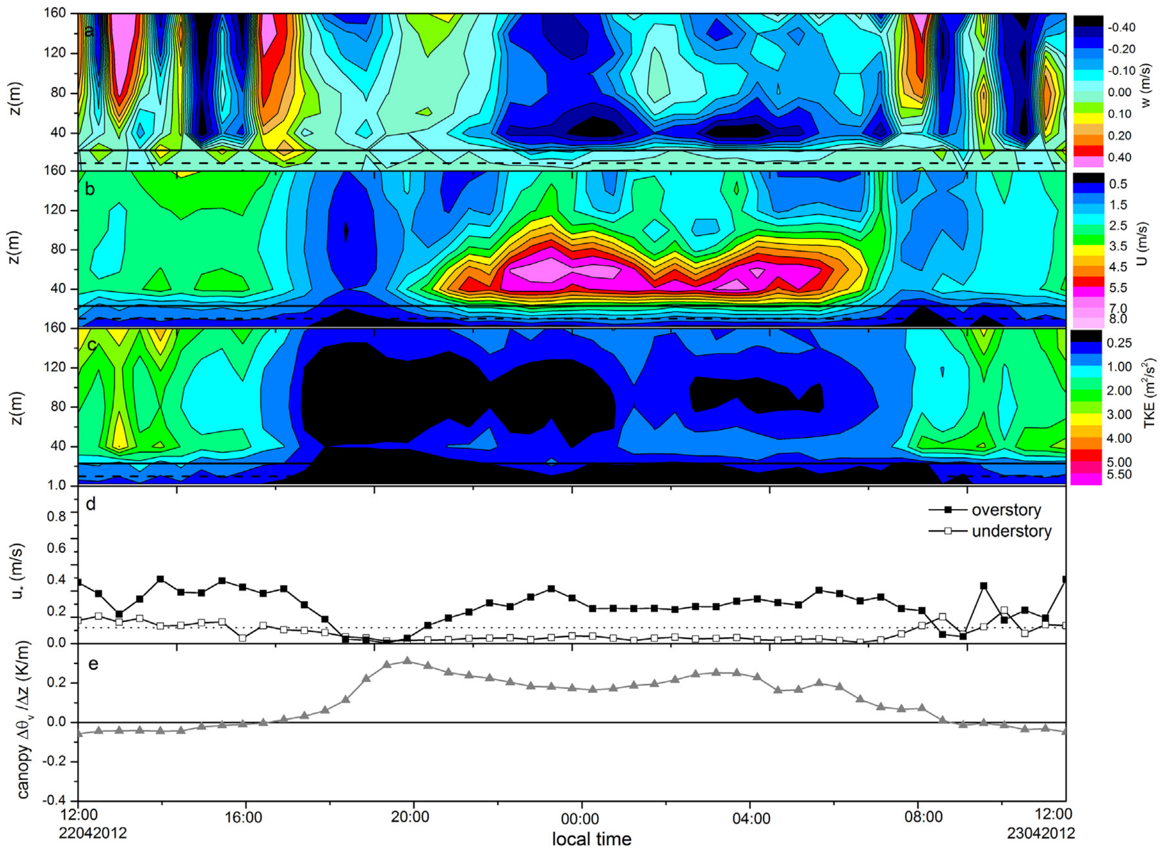

Fig. 4. Same as Fig. 3 except a typical nighttime downslope flow event is shown at Tonzi on the night of 22–23 April 2012.

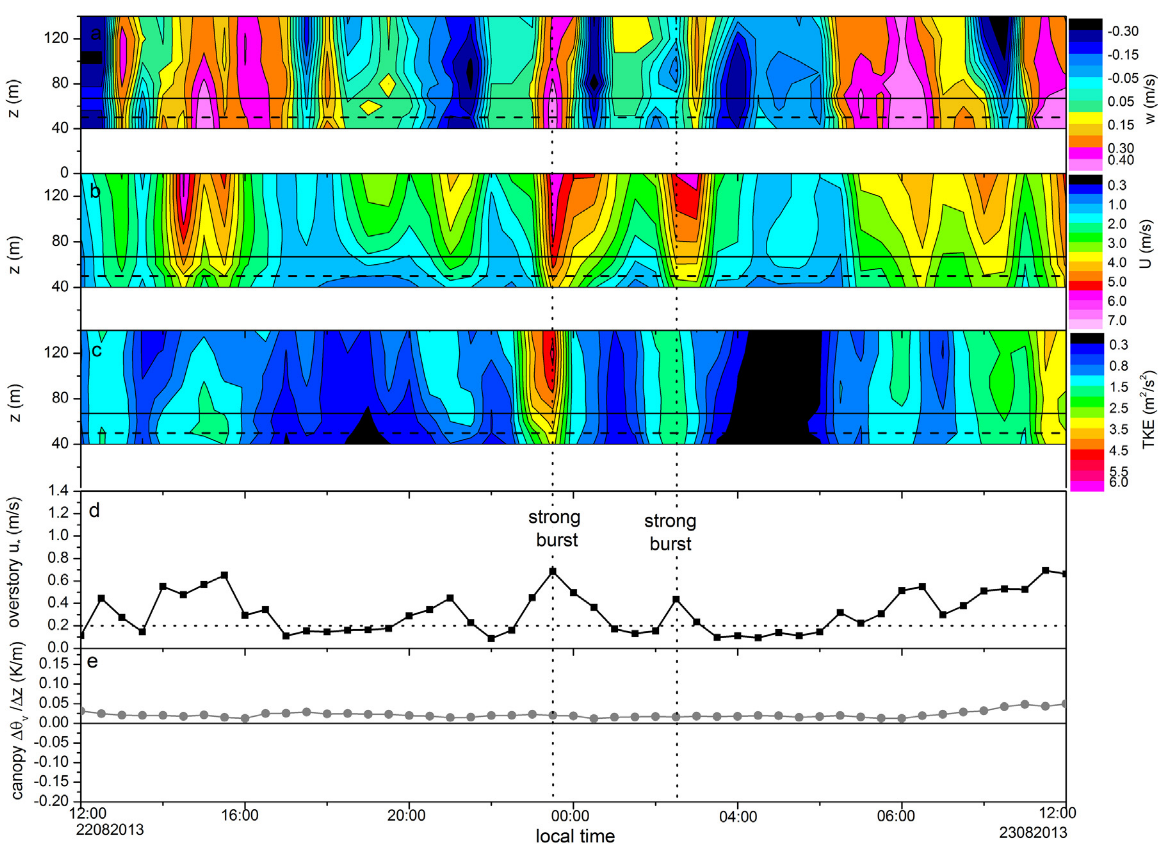

Fig. 5. A typical strong top-down forced turbulence event at Wind River. The night of 22–23 August 2013 is plotted.

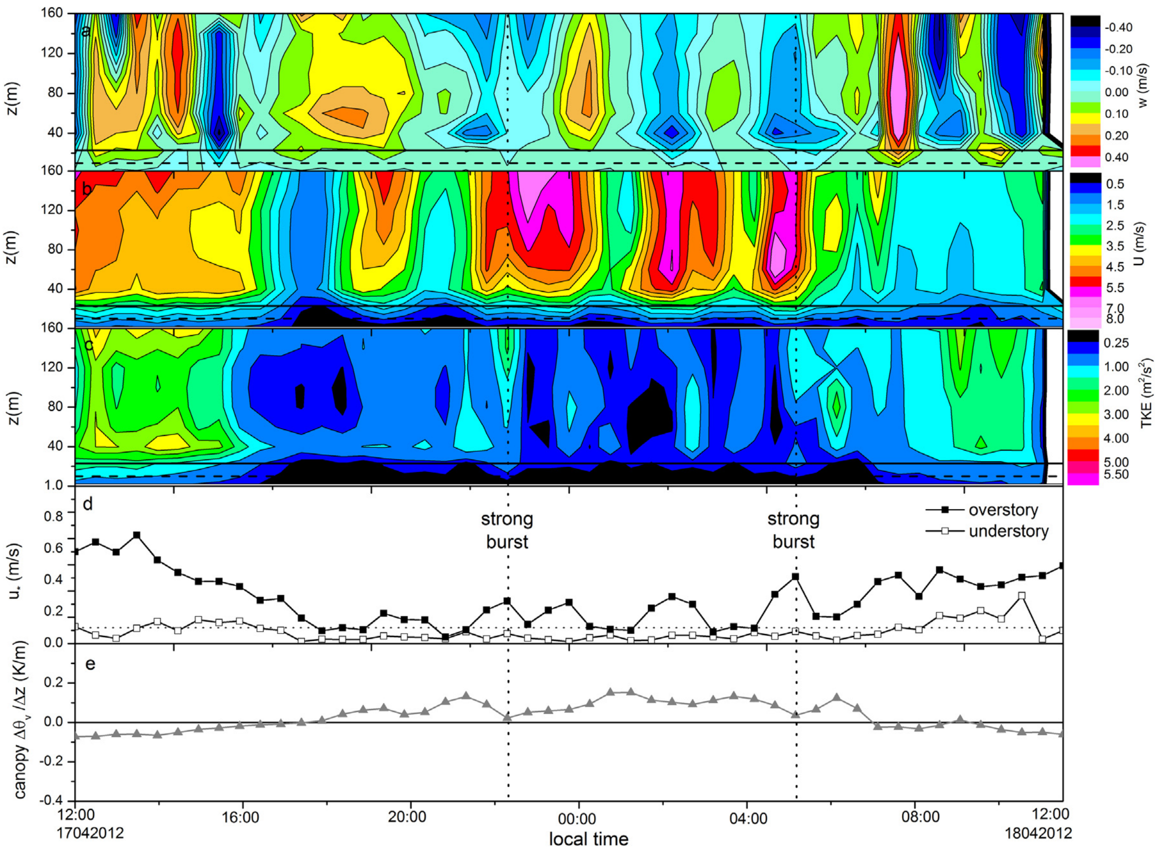

Fig. 6. A typical strong top-down forced turbulence event at Tonzi. The night of 17–18 April 2012 is plotted.

and 3rd Quartile for downslope and "top-down" forced turbulence events, respectively. Moreover, the ratios of canopy $\sigma_w < 0.2$ observed during downslope flows (driven by smaller values of understory σ_w) also confirm this finding of canopy decoupling (Fig. 7b). Furthermore, *[CO_2]* profile measurements taken along the tower indicated larger gradients on downslope nights (not shown), particularly between the heights of 1.8–6 m, suggesting that the sub-canopy air space is largely decoupled from the air above during these events.

To look more closely at how static stability is related to each of the turbulence parameters, we plotted them against $\Delta\theta_v/\Delta z$ in Fig. 9. The panels are separated into four quadrants based on the canopy coupling threshold for $\Delta\theta_v/\Delta z$ (y-axis) and the turbulence threshold for the four turbulence parameters (x-axis). Half-hours that have both a weak canopy temperature gradient (i.e., $\Delta\theta_v/\Delta z$ <0.15) and high turbulence parameter are found in quadrant *iv*. Likewise, half-hours that have both a large $\Delta\theta_v/\Delta z$ and a low turbulence parameter value are found in quadrant *ii*. Fig. 9 shows that the majority of half-hours taken during top-down forced turbulence nights fall into quadrant *iv*, implying a relationship between weaker canopy stability and higher turbulence. However, this relationship falters during downslope flow events. For example, Fig. 9a shows a potential error that may arise from using overstory u_* as a proxy for the magnitude of canopy turbulent exchange during downslope flow. A strong discrepancy was found on these nights between $\Delta\theta_v/\Delta z$, which was large and intuitively suggests that the nighttime canopy air is poorly mixed, and overstory u_*, which was enhanced and intuitively suggests high turbulent mixing in the open canopy. During downslope flow u_* was greater than u_{*crit} 73% of the time (points in quadrant *iii* and *iv* in Fig. 9a) suggesting conditions favorable for high turbulent transfer, yet 97% of the half hours also saw conditions when the canopy potential temperature gradient was strong and larger than our prescribed threshold (0.15 K/m). In contrast, during top-down forced turbulence events u_* had similar values ($u_* > u_{*crit}$ 73% of the time) as during downslope flows, yet $\Delta\theta_v/\Delta z$ was much weaker and the number of half hours which exceeded the $\Delta\theta_v/\Delta z$ threshold (0.15 K/m) dropped to 28%.

When R_{igr} is less than R_c (0.25), the canopy layer is traditionally described as dynamically unstable. These conditions occurred 26% of the time for top-down forced turbulence events but less than 1% of the time during downslope flows (Fig. 9d). On the other hand, a larger number of half-hours were classified as dynamically stable during downslope flows. This partially explains the weak correlation between overstory u_* and the canopy temperature gradient in Fig. 9a. For half hours when $0.25 < R_{igr} < 1$ (i.e., $R_{c<}\ R_{igr<}\ R_T$), the data points are clearly segregated according to atmospheric regime in a similar manner as they are for u_*. Such that for any given R_{igr} value within this range, $\Delta\theta_v/\Delta z$ is largely above the canopy coupling threshold during downslope flows (implying decoupled flow) and largely below on top-down forced turbulence nights (implying coupled flow). A different relationship between turbulence and $\Delta\theta_v/\Delta z$ on downslope nights is seen from using the alternative turbulence parameters based on variance, $\sigma_{wunderstory}/\sigma_{woverstory}$ and I_{TKE}. In contrast to u_*, smaller values of these turbulence parameters correspond to times with larger temperature gradients. In comparison to Fig. 9a, in b and c a greater proportion of the downslope data points have now shifted from quadrant *iii* to *ii* where conditions show both weak turbulence and higher static stability.

There is an increasing amount of evidence that suggests that canopy stratification and turbulence intensity is far more complicated in the nocturnal boundary layer than originally thought (e.g., Sun et al., 2012; Hicks et al., 2014, Liang et al., 2014, Mahrt and Thomas, 2016). For example, Vickers and Mahrt (2007) and Acevedo et al. (2009) found that mesoscale motions show little relationship

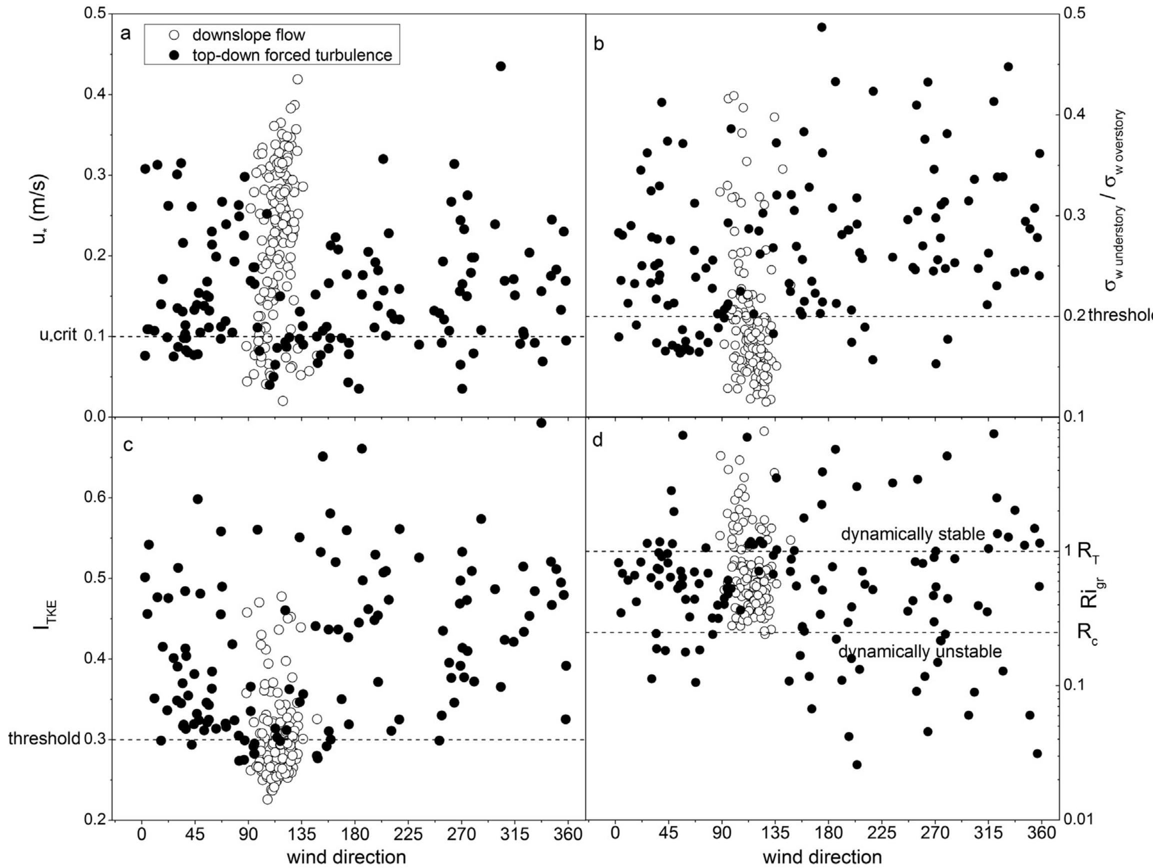

Fig. 7. The four turbulence parameters plotted as a function of overstory wind direction at Tonzi. The dotted lines are thresholds for each parameter based on published values for u_* and Ri_{gr} and the median value of *understory* σ_w*/overstory* σ_w and I_{TKE}. The half-hourly data points are segregated into downslope and top-down forced turbulence events.

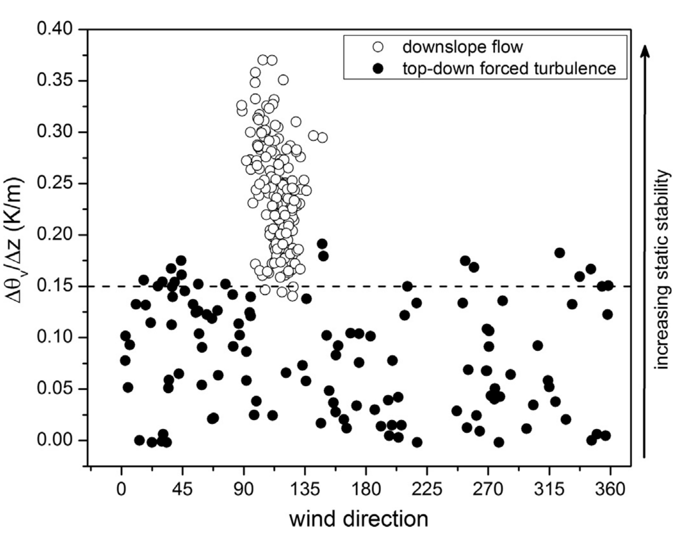

Fig. 8. Half-hourly values of canopy virtual potential temperature gradient plotted by overstory wind direction at Tonzi. Canopy mixing strength was assumed to be proportional to $\Delta\theta_v/\Delta z$ such that gradients >0.15 K/m approach canopy flow decoupling and <0.15 K/m approach canopy flow coupling. The dotted line indicates the hypothetical canopy coupling threshold.

to local scaling variables including friction velocity, and significant temperature gradients have been observed despite the presence of enhanced turbulence (Mahrt and Thomas, 2016). The lack of uniformity between our turbulence parameters and $\Delta\theta_v/\Delta z$ during regional downslope flow appears to corroborate the theory that the relationship between turbulence and stable stratification is less systematic than once assumed.

5. Conclusions

At Tonzi and Wind River two regional nighttime flow events were measured above the canopy: down-valley or downslope flow and top-down forced turbulence. At Wind River, down-valley flows were associated with very low values of turbulence above the canopy. Shear and turbulence values were greatest during top-down forced turbulence events. While the overstory station at Wind River measured discernable differences in wind flow and turbulence statistics on nights with down-valley flow versus top-down forced turbulence events, a lack of observational change in the potential temperature and $[CO_2]$ gradients was present. We suggest two possible reasons: (1) the tall, high biomass canopy acts as a strong mechanical barrier to downward momentum, resulting in strong flow decoupling between the sub-canopy, canopy, and air above even during the strongest turbulent burst events, or (2) changes in mid-canopy or sub-canopy gradients did occur but were not observable given our limited number of instruments within the canopy.

At Tonzi, bursts of top-down forced turbulence appeared to penetrate the oak-savannah canopy down to significant depths (down to 2 m a.g.l. or more) as we observed weaker vertical gradients of θ_v and $[CO_2]$ within the canopy, and elevated turbulence in the sub-canopy. One of the most important insights from the lidar field campaigns was the observation that there are a significant number of times at Tonzi when nighttime u_* is high and well above the site's critical threshold for determining sufficient turbulence, yet tem-

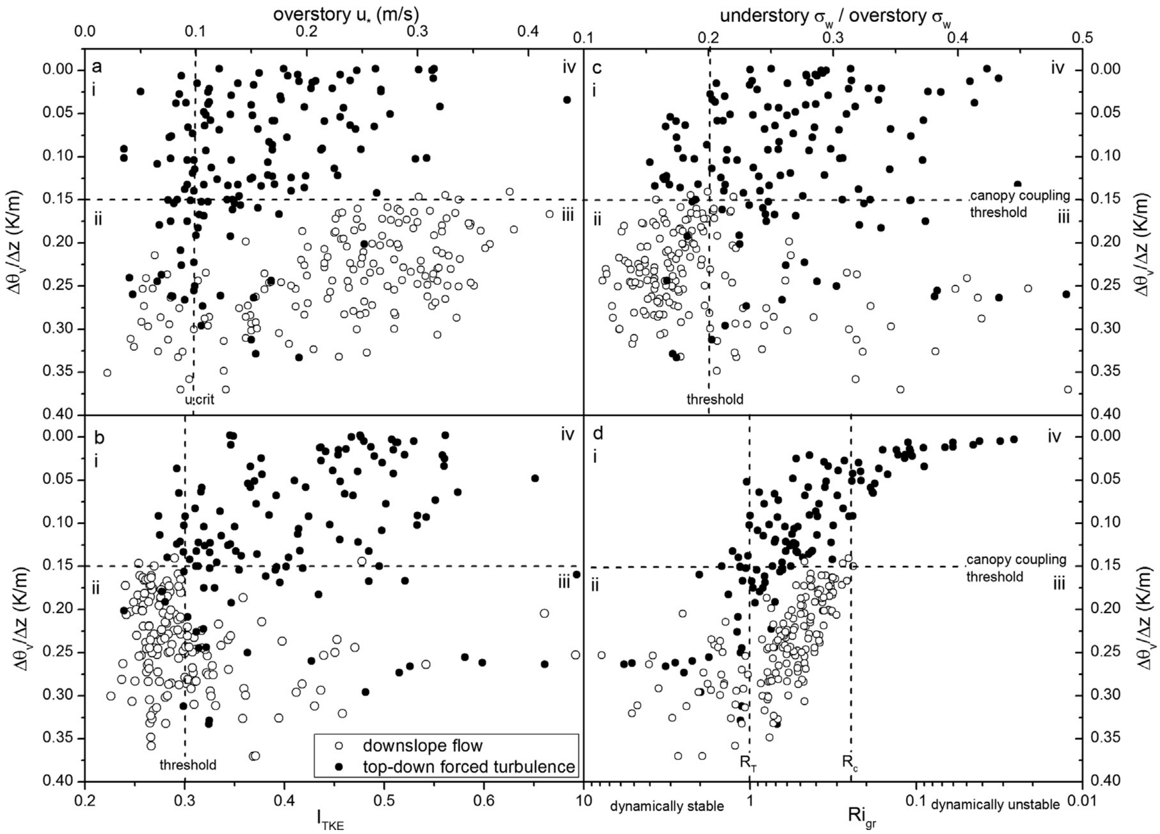

Fig. 9. Half-hourly canopy virtual potential temperature gradients plotted against the set of turbulence parameters according to nighttime flow event. Each panel is divided into four quadrants (*i*–*iv*) such that data in quadrant ii fail both the turbulence parameter threshold and $\Delta\theta_v/\Delta z$ threshold (dotted lines), and data in quadrant *iv* surpass both thresholds. For example, half-hours that have a u_* value above u_{*crit} (>0.1 m/s), and indicate high above-canopy turbulence conditions, and a $\Delta\theta_v/\Delta z$ value that indicates possible canopy coupling (<0.15 K/m) are found in panel a quadrant *iv*.

perature and scaler gradients suggest that the canopy may strongly decoupled. These conditions were a distinct feature of downslope flow events and although this non-local flow was hypothesized to occur at the site, it had not been detected prior the lidar deployments and its impacts on canopy gradients and canopy mixing were unknown.

During downslope flows turbulence parameters based on overstory u_* and wind shear (i.e., R_{igr}) proved to be inaccurate metrics for estimating turbulence found within the canopy. This suggests that the u_* correction method is inappropriate during these strong nonlocal flow events. This finding adds further corroboration to studies pointing out the limitations of using overstory u_* as a canopy turbulence threshold (Gu et al., 2005; Acevedo et al., 2009; Wharton et al., 2009; Thomas et al., 2013; Vickers and Thomas, 2013). Alternative statistics based on variance in the form of vertical velocity variance or ratio of 3-D turbulence to mean flow appeared to better estimate canopy flow conditions at the open canopy. However, after examining all four turbulence parameters it is apparent that the relationship between turbulence strength and canopy stability is far from straightforward. This topic deserves further attention at Tonzi, and at other open and closed canopies, and would require profile measurements with greater resolution and precision than found here.

Acknowledgements

The authors would like to thank Joe Verfaillie (Tonzi) and Matt Schroeder (Wind River) for their help with the EC systems, lidar deployments, and other site logistics. Thanks go to Maureen Alai, Cary Gellner, Jeff Mirocha, Katie Myers, and John van Fossen (LLNL) for their help with setting up the lidars and to MA, CG, and JVF for building the solar/battery power units that were used at Tonzi. Additional gratitude goes to Dave Hollinger (USDA Forest Service) for providing the Wind River CO_2 profile data. This research was supported by a LLNL Laboratory Directed Research and Development (LDRD) award Grant No. 12-ERD-043. On-going support for Tonzi, a Core AmeriFlux Site, was provided by the U.S. Department of Energy's Office of Science.

The Wind River AmeriFlux Field Station operates from an agreement among the University of Washington, the Pacific Northwest Research Station (PNW), and the Gifford Pinchot National Forest. Lawrence Livermore National Laboratory is operated by Lawrence Livermore National Security, LLC, for the US Department of Energy, National Nuclear Security Administration under Contract DE-AC52-07NA27344.

References

Acevedo, O.C., Fitzjarrald, D.R., 2003. In the core of the night-effects of intermittent mixing on horizontally heterogeneous surfaces. Bound.-Layer Meteor. 106, 1–33.

Acevedo, O.C., Moraes, O.L., Degrazia, G.A., Fitzjarrald, D.R., Manzi, A.O., Campos, J.G., 2009. Is friction velocity the most appropriate scale for correcting nocturnal carbon dioxide fluxes? Agric. For. Meteor. 149, 1–10.

Baldocchi, D.D., Tang, J., Xu, L., 2006. How switches and lags in biophysical regulators affect spatial-temporal variation of soil respiration in an oak-grass savanna. J. Geophys. Res. 111, G02008, http://dx.doi.org/10.1029/2005JG000063.

Baldocchi, D.D., Ma, S., Rambal, S., Misson, L., Ourcival, J.-M., Limousin, J.-M., Pereira, J., Papale, D., 2010. On the differential advantages of evergreenness and deciduousness in Mediterranean oak woodlands: a flux perspective. Ecol. Appl. 20 (6), 1583–1597.

Businger, J., 1973. Turbulent transfer in the atmospheric surface layer. In: Haugen, D. (Ed.), Workshop on the Planetary Boundary Layer. Am. Met. Soc., pp. 67–98.

Cañadillas, B., Bégué, A., Neumann, T., 2010. Comparison of turbulence spectra derived from LiDAR and sonic measurements at an offshore platform FINO1. In: DEWEK 2010 10th German Wind Energy Conference, Bremen, Germany.

Cariou, J.P., Boquet, M., 2011. Leosphere Pulsed Lidar Principles Contribution to Upwind WP6 on Remote Sensing Devices. Leosphere, Orsay, France http://www.upwind.eu/media/576/D6.1.1.pdf.

Choi, W., Faloona, I.C., McKay, M., Goldstein, A.H., Baker, B., 2011. Estimating the atmospheric boundary layer height over sloped, forested terrain from surface spectral analysis during BEARPEX. Atmos. Chem. Phys. 11, 6837–6853.

Dellwik, E., Mann, J., Larsen, K.S., 2010. Flow tilt angles near forest edges – Part 2: lidar anemometry. Biogeosciences 7, 1759–1768.

El-Madany, T.S., Duarte, H.F., Durden, D.J., Paas, B., Deventer, M.J., Juang, J.-Y., Leclerc, M.Y., Klemm, O., 2014. Low-level jets and above-canopy drainage as causes of turbulent exchange in the nocturnal boundary layer. Biogeosciences 11, 4507–4519.

Falk, M., Paw U, K.T., Wharton, S., Schroeder, M., 2005. Is soil respiration a major contributor to the carbon budget within a Pacific Northwest old-growth forest? Agric. For. Meteorol. 135, 269–283.

Falk, M., Wharton, S., Schroeder, M., Ustin, S., Paw U, K.T., 2008. Flux partitioning in an old-growth forest: seasonal and interannual dynamics. Tree Physiol. 28, 509–520.

Froelich, N., Schmid, H.P., 2006. Flow divergence and density flows above and below a deciduous forest. Part II: below-canopy topographic flows. Agric. For. Meteorol. 138, 29–43.

Goulden, M.L., Munger, J.W., Fan, S.M., Daube, B.C., Wofsy, S.C., 1996. Exchange of carbon dioxide by a deciduous forest: response to interannual climate variability. Science 271, 1576–1578.

Gu, L., Falge, E.M., Boden, T., Badocchi, D.D., Black, T.A., Saleska, S.R., Suni, T., Verma, S.B., Vesala, T., Wofsy, S.C., Xu, L., 2005. Objective threshold determination for nighttime eddy flux filtering. Agric. For. Meteorol. 128, 179–197.

Harmon, M.E., Bible, K., Ryan, M.G., Shaw, D.C., Chen, H., Klopatek, J., Li, X., 2004. Production respiration, and overall carbon balance in an old-growth *Pseudotsuga-Tsuga* forest ecosystem. Ecosystems 7, 498–512.

Karipot, A., Leclerc, M.Y., Zhang, G., Lewin, K.F., Nagy, J., Hendrey, G.R., Starr, G., 2008. Influence of nocturnal low-level jet on turbulence structure and CO_2 flux measurements over a forest canopy. J. Geophys. Res. 113, D10102, http://dx.doi.org/10.1029/2007JD009149.

Krishnamurthy, R., Boquet, M., 2014. Case studies of WINDCUBE measurement uncertainty for complex terrain using flow complexity recognition (FCR). In: EWEA Conference, Barcelona, Spain.

Ma, S., Baldocchi, D.D., Xu, L., Hehn, R., 2007. Interannual variability in carbon dioxide exchange of an oak/grass savanna and open grassland in California. Agri. For. Meteorol. 147, 151–171.

Mahrt, L., Thomas, C.K., 2016. Surface stress with non-stationary weak winds and stable stratification. Bound.-Layer Meteor. 159, 3–21.

Mahrt, L., 1989. Intermittency of atmospheric turbulence. J. Atmos. Sci. 46, 79–95.

Mahrt, L., 1999. Stratified atmospheric boundary layers. Bound.-Layer Meteor. 90, 375–396.

Mann, J., Dellwik, E., Bingöl, F., Rathman, O., 2008. Laser measurements of flow over a forest. 14th International Symposium for the Advancement of Boundary Layer Remote Sensing, IOP Conf. Series: Earth and Environmental Science 1, http://dx.doi.org/10.1088/1755-1307/1/1/012050.

Morgan, D.L., Slusser, W.F., 1978. A pilot study of upslope winds in the Sierra Nevada. In: Conference on Sierra Nevada Meteorology (Preprint Volume), Boston, American Meteorological Society, pp. 83–90.

Newman, J.F., Klein, P.M., Wharton, S., Sathe, A., Bonin, T.A., Chilson, P.B., Muschinski, A., 2016. Evaluation of three lidar scanning strategies for turbulence measurements. Atmos. Meas. Technol. 9, 1993–2013.

Parker, G.G., Davis, M.M., Chapotin, S.M., 2002. Canopy light transmittance in Douglas-fir-western-hemlock stands. Tree Physiol. 22, 147–157.

Paw U, K.T., Falk, M., Suchanek, T.H., Ustin, S.L., Chen, J., Park, Y.-S., Winner, W.E., Thomas, S.C., Hsiao, T.C., Shaw, R.H., King, T.S., Pyles, R.D., Schroeder, M., Matista, A., 2004. Carbon dioxide exchange between an old-growth forest and the atmosphere. Ecosystems 7, 513–524.

Pyles, R.D., Paw U, K.T., Falk, M., 2004. Directional wind shear within an old-growth temperate rainforest: observations and model results. Agric. For. Meteor. 125, 19–31.

Rotach, M., Andretta, M., Calanca, P., Weigel, A., Weiss, A., 2008. Boundary layer characteristics and turbulent exchange mechanisms in highly complex terrain. Acta Geophys. 56, 194–219.

Ryu, Y., Sonnentag, O., Nilson, T., Vargas, R., Kobayashi, H., Wenk, R., Baldocchi, D., 2010. How to quantify tree leaf area index in an open savanna ecosystem: a multi-instrument and multi-model approach. Agric. For. Meteor. 150, 63–76.

Sathe, A., Mann, J., 2012. Measurement of turbulence spectra using scanning pulsed wind lidars. J. Geophys. Res.: Atmos. 117, D01201.

Sathe, A., Mann, J., 2013. A review of turbulence measurements using ground-based wind lidars. Atmos. Meas. Technol. 6, 3147–3167.

Shaw, D.C., Franklin, J.F., Bible, K., Klopatek, J., Freeman, E., Greene, S., Parker, G.G., 2004. Ecological setting of the Wind River old-growth forest. Ecosystems 7, 427–439.

Slinger, C., Harris, M., 2012. Introduction to continuous-wave Doppler lidar. In: Proceedings of the Summer School in Remote Sensing for Wind Energy, 11–15 June 2012, Boulder, Colorado (32 p.).

Smith, C.M., Porté-Agel, F., 2014. An intercomparison of subgrid models for large-eddy simulation of katabatic flows. Q. J. Royal Meteor. Soc. 140, 1294–1303.

Strauch, R.G., Merritt, D.A., Moran, K.P., Earnshaw, K.B., De Kamp, D.V., 1984. The colorado wind-profiling network. J. Atmos. Ocean. Technol. 1, 37–49.

Stull, R.B., 1988. An Introduction to Boundary Layer Meteorology. Kluwer Academic Publishers, The Netherlands (670 p.).

Sun, J., Mahrt, L., Banta, R.M., Pichugina, Y.L., 2012. Turbulence regimes and turbulence intermittency in the stable boundary layer during CASES-99. J. Atmos. Sci. 69, 338–351.

Thomas, S.C., Winner, W.E., 2000. Leaf area index of an old-growth Douglas-fir forest estimated from direct structural measurements in the canopy. Can. J. For. Res. 30, 1922–1930.

Thomas, C.K., Mayer, J.-C., Meixner, F.X., Foken, T., 2006. Analysis of low-frequency turbulence above tall vegetation using a Doppler sodar. Bound.-Layer Meteor. 119, 563–587.

Thomas, C.K., Martin, J.G., Law, B.E., Davis, K., 2013. Toward biologically meaningful net carbon exchange estimates for tall, dense canopies: multi-level eddy covariance observations and canopy coupling regimes in a mature Douglas-fir forest in Oregon. Agric. For. Meteor. 173, 14–27.

Vickers, D., Mahrt, L., 2006. A solution for flux contamination by mesoscale motions with very weak turbulence. Bound.-Layer Meteor. 118, 431–447.

Vickers, D., Mahrt, L., 2007. Observations of the cross-wind velocity variance in the stable boundary layer. Environ. Fluid Mech. 7, 55–71.

Vickers, D., Thomas, C.K., 2013. Some aspects of the turbulence kinetic energy and fluxes above and beneath a tall open pine canopy. Agric. For. Meteor. 181, 143–151.

Wang, X., Wang, C., Li, Q., 2015. Wind regimes above and below a temperate deciduous forest canopy in complex terrain: interactions between slope and valley winds. Atmosphere 6, 60–87.

Wharton, S., Schroeder, M., Paw U, K.T., Falk, M., Bible, K., 2009. Turbulence considerations for comparing ecosystem exchange over old-growth and clear-cut stands for limited fetch and complex canopy flow conditions. Agric. For. Meteor. 149, 1477–1490.

Wharton, S., Falk, M., Bible, K., Schroeder, M., Paw U, K.T., 2012. Old-growth CO_2 flux measurements reveal high sensitivity to climate anomalies across seasonal, annual and decadal time scales. Agric. For. Meteor. 161, 1–14.

Whiteman, C.D., Zhong, S.-Y., 2008. Downslope flows on a low-angle slope and their interactions with valley inversions. Part 1: observations. J. Appl. Meteor. Climatol. 47, 2023–2038.

Xu, L., Baldocchi, D.D., 2003. Seasonal trend of photosynthetic parameters and stomatal conductance of blue oak (*Quercus douglasii*) under prolonged summer drought and high temperature. Tree Physiol. 23, 865–877.

Yi, C., Monson, R.K., Zhai, Z., Anderson, D.E., Lamb, B., Allwine, G., Turnipseed, A.A., Burns, S.P., 2005. Modeling and measuring the nocturnal drainage flow in a high-elevation, subalpine forest with complex terrain. J. Geophys. Res.: Atmos. 110, http://dx.doi.org/10.1029/2005jd006282.

Yi, C., Anderson, D.E., Turnipseed, A.A., Burns, S.P., Sparks, J.P., Stannard, D.I., Monson, R.K., 2008. The contribution of advective fluxes to net ecosystem exchange in a high-elevation, subalpine forest. Ecol. Appl. 18 (6), 1379–1390.

van de Wiel, B., Ronda, R., Moene, A., de Bruin, H., Holtslag, A., 2002. Intermittent turbulence and oscillations in the stable boundary layer over land. Part 1: a bulk model. J. Atmos. Sci. 59, 942–958.